

## Long- to short-junction crossover and field-reentrant critical current in Al/Ag-nanowires/Al Josephson junctions

A. Murani,<sup>1,2</sup> S. Sengupta,<sup>1,3</sup> A. Kasumov,<sup>1,4</sup> R. Deblock,<sup>1</sup> Caroline Celle,<sup>5</sup> J-P. Simonato,<sup>5</sup> H. Bouchiat,<sup>1</sup> and S. Guéron<sup>1</sup>

<sup>1</sup>Laboratoire Université Paris-Saclay, CNRS, Laboratoire de Physique des Solides, 91405 Orsay, France

<sup>2</sup>Quantronics Group, Service de Physique de l'Etat Condensé (CNRS UMR 3680), IRAMIS, CEA-Saclay, 91191 Gif-sur-Yvette, France

<sup>3</sup>Université Paris-Saclay, CNRS/IN2P3, IJCLab, 91405 Orsay, France

<sup>4</sup>Institute of Microelectronics Technology and High Purity Materials RAS, 6, Academician Ossipyan str., Chernogolovka, Moscow Region 142432, Russia

<sup>5</sup>Université Grenoble Alpes, CEA, LITEN DTNM, F-38054 Grenoble, France



(Received 6 November 2019; revised 13 October 2020; accepted 28 October 2020; published 16 December 2020)

We have probed the superconducting proximity effect through long high-quality monocrystalline Ag nanowires, by realizing Josephson junctions of different lengths, with different superconducting materials. Thanks to the high number of junctions probed, both the contact resistance and electron diffusion constant could be determined, enabling a comparison of the measured switching current to theoretical prediction, over the entire regime from short to long diffusive junctions. Although the length dependence of the switching current is as expected, the amplitude of the  $R_N I_c$  product is smaller than predicted by theory. We also address the magnetic field dependence of the switching current. The quasi-Gaussian decay of the switching current with field expected in a long narrow junction is observed for all superconducting contacts we used except for aluminum. We present the striking nonmonotonous effect of field on the switching current of junctions with aluminum contacts when probed in a four-wire configuration and analyze it in terms of improved quasiparticle thermalization by a magnetic field.

DOI: [10.1103/PhysRevB.102.214506](https://doi.org/10.1103/PhysRevB.102.214506)

### I. INTRODUCTION

The superconducting proximity effect, in which a superconductor (S) confers superconductinglike properties to a nonsuperconducting (also called “normal,” N), quantum coherent, material connected to it, is epitomized by the fact that a supercurrent can flow through an S/N/S junction. The critical current, or maximal supercurrent, is a measure of the characteristic energy of the junction. It is related either to the superconductor’s energy gap  $\Delta$ , or to the Thouless energy, associated to the inverse dwell time in the normal metal:  $R_N I_c \propto \min(\Delta, \hbar D_N/L^2)$  [1–3], where  $D_N$  is the diffusion constant and  $L$  the length of the normal segment. This relation between critical current and characteristic energies was quantitatively tested over a wide parameter range for diffusive S/graphene/S junctions [4], and qualitatively tested very recently in S/InSb quantum wells/S junctions [5]. In Ref. [4], the tunability of graphene was used to vary  $D_N$  with a gate voltage in order to probe the relation. In the present paper, rather than varying the diffusion constant, we rely on high quality monocrystalline Ag wires of remarkably constant properties [6–8] (diameters, diffusion constant, contact resistance) to probe this relation. To this end, we have measured the supercurrent induced through almost twenty Ag nanowire segments, whose lengths range between 200 nm and 5 microns, sampling the regimes from short to long SNS junctions, with an almost three order of magnitude range of the Thouless energy. In contrast to the S/graphene/S junctions, that were

several micrometers wide, the S/Ag/S junctions are narrow, with a Ag wire diameter of roughly 50 nm. This has several consequences, in particular the field dependence of the critical current is drastically different. For most superconducting contacts we tried (Pd/Nb, W, Pd/ReW), we find a monotonously decaying critical current as the magnetic field is increased, as is expected of long narrow junctions [9–11]. For Al contacts however we find that the magnetic field increases the critical current at low fields, when the junction is measured in a four-wire configuration. We interpret this in terms of a positive role of magnetic field for quasiparticle thermalization, a sensitive issue in narrow metallic wires [12]. Our findings have implications on understanding experiments with aluminum as the superconductor, for instance experiments on nanowires with spin-orbit interactions connected to aluminum electrodes, in which the magnetic field behavior is a key for the identification of a topological transition and the search for Majorana fermions [13]. These findings may also be important to understand quasiparticle poisoning processes and their field dependence in proximity systems and superconducting circuits [14].

### II. SAMPLE FABRICATION

The synthesis of Ag nanowires was performed according to a recently published protocol, developed for the production of transparent electrodes based on nanowire random networks

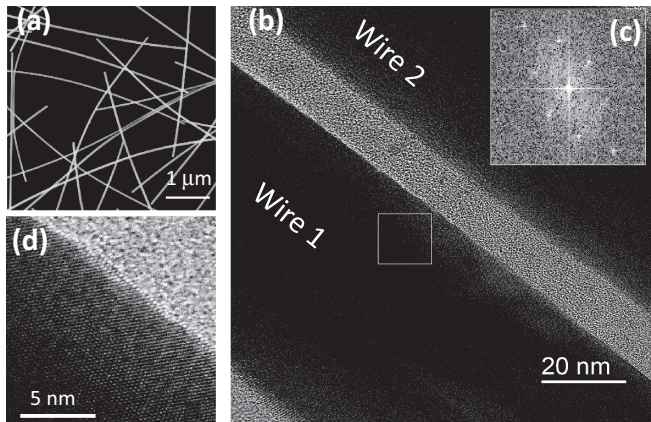


FIG. 1. Imaging the Ag nanowires. (a) Scanning electron micrograph (SEM). (b) Bright field scanning transmission electron micrograph (STEM) of two Ag nanowires such as those measured. The fast Fourier transform of the zone indicated by the white square is shown in (c), demonstrating the high crystallinity of the wires. Interestingly, the two parallel wires, labeled Wire 1 and Wire 2, have the same crystalline orientation (not shown). (d) Higher-magnification, atomic-resolution, STEM image.

[6]. In order to enhance induced superconductivity through the wires, a highly purified source of  $\text{AgNO}_3$  (purity 99.9999%) was used in the present synthesis. Briefly, the synthesis consists in the reduction of silver salt through a polyol process and the purification is realized by a two-step decantation procedure. The sheet resistance of a spraycoated network of these nanowires was  $20 \Omega/\text{sq}$  at 90% transparency (measured at 550 nm). The nanowires grow along the [111] direction. The diameter was typically 50 nm, as determined by STEM and SEM characterizations, see Fig. 1. STEM observation are also compatible with a fivefold symmetry and a highly strained core.

To isolate individual nanowires, a drop of a highly diluted solution of these nanowires in VLSI methanol is deposited on an oxide covered silicon substrate. Nanowires are selected in an optical microscope, using a polarizer to enhance contrast. Contacts are defined by electron-beam lithography, and the superconducting materials are deposited by either e-gun evaporation (Ti/Al with thickness 5 nm/100 nm), dc sputtering (Pd/Nb or Pd/ReW, thicknesses 6 nm/100 nm), or focused-ion-beam (FIB)-assisted deposition (W-based compound, of thickness about 100 nm). The quality of the contacts between the silver nanowire and the superconductor is enhanced by a prior *in situ* argon ion etching step in the case of e-gun or sputter deposition. FIB-assisted deposition, by contrast, requires no additional etching step, for W deposition is induced by Ga-ion-assisted decomposition of a hexacarbonyl W gas and is concomitant to a slight etching of the Ag wire by the Ga ions. In fact, we find that FIB-assisted-deposition of superconducting contacts is particularly suited to contact wires covered by an insulating oxide [15]. In the following, we focus on Ag nanowires connected to Ti/Al electrodes, since they produce the most reliable results and the striking field dependence that we wish to address.

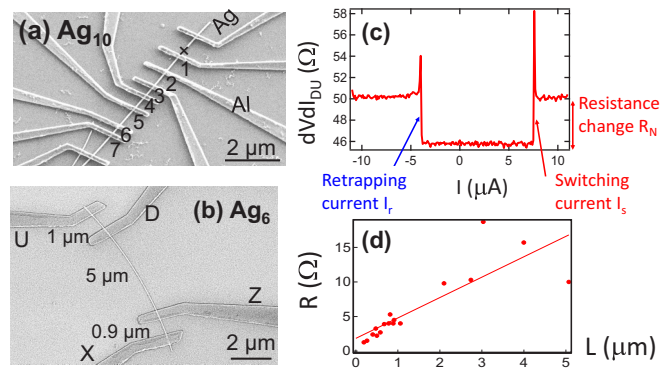


FIG. 2. Diffusive transport in Ag nanowires. The scanning electron micrograph of two of the wires, Ag6 and Ag10, with TiAl contacts, are displayed in (a) and (b). (c) Differential resistance as a function of dc current of sample TiAl Ag6-DU, measured at  $T \simeq 100$  mK, in a two wire configuration. The  $46 \Omega$  resistance corresponds to the series resistance of the wires running from room temperature down to the sample at mK temperature. As the current is swept from negative to positive, the resistance of the segment itself is zero for a current between  $-4 \mu\text{A}$ , the retrapping current  $I_r$ , and  $7.5 \mu\text{A}$ , the switching current  $I_s$ . The resistance change of  $4 \Omega$  at the switching current is the normal state resistance of the segment  $R_N$ . (d) Normal resistance of 17 segments from eight Ag nanowires with Ti/Al superconducting contacts. The linear increase of resistance with segment length indicates a diffusive behavior from 100 nm to 5 microns. The contact resistance and resistance per micron deduced from a linear fit to the data (continuous line) are  $1.8 \pm 1 \Omega$  and  $3 \pm 1 \Omega/\mu\text{m}$  respectively, yielding a resistivity of  $6 \pm 2 \cdot 10^{-9} \Omega\text{m}$ , assuming that all the wires have a diameter of 50 nm. This resistivity is similar to that measured in Refs. [7,18].

### III. MEAN FREE PATH AND CONTACT RESISTANCE DETERMINATION

The wire resistivity and contact resistances were determined by probing several Ag segments of different lengths with the superconducting proximity effect. Indeed the resistance jump as the junctions switches from a (proximity-induced) superconducting state with zero resistance to a resistive state as the current exceeds the critical current (see Fig. 2), gives the normal resistance  $R_N$  of the segment. Plotting  $R_N$  as a function of the Ag segment length thus yields the parameters characterizing the transport regime (contact resistance and elastic mean free path). Figure 2 displays the variation of the normal state resistance with segment length of 17 segments from eight Ag nanowires, connected to Ti/Al superconducting contacts. The linear dependence indicates that the transport regime is diffusive, and yields the contact resistance, mean free path, and wire resistivity. Indeed the length dependence of the resistance can be written as  $R(L) = 2R_c + \frac{R_Q}{M} \frac{L}{l_e}$ , where  $R_c$  is the contact resistance at each interface,  $R_Q = h/2e^2$  the resistance quantum for a spin degenerate channel,  $L$  the wire length,  $l_e$  the elastic mean free path, and  $M$  the number of channels. The contact resistance of each channel has two contributions: in addition to the Sharvin (or access) resistance  $R_Q$ , which yields  $R_Q/M$  for  $M$  channels, each channel can be partially transmitted at the contact, with a transmission coefficient  $\tau$ , causing an additional resistance

$\frac{1-\tau}{\tau}$  [16,17]. Therefore, if we assume that all channels have the same transmission coefficient, we find that twice the contact resistance reads  $2R_c = \frac{R_Q}{M} (1 + \frac{1-\tau}{\tau}) = \frac{R_Q}{M} \frac{1}{\tau}$ , so that  $R(L) = \frac{R_Q}{M} (\frac{1}{\tau} + \frac{L}{l_e})$  [16,17].

In a 3D system of section  $S$  and Fermi wave vector  $k_F$ ,  $M = k_F^2 S / (4\pi)$ . Given the diameter  $d = 50$  nm and Ag's Fermi wave vector  $k_F = 1.2 \times 10^{10} \text{ m}^{-1}$ , we find  $M \simeq 2 \times 10^4$  channels. The slope of  $3 \text{ } \Omega/\mu\text{m}$  thus corresponds to a resistivity  $\rho = (R - 2R_c)S/L \simeq 6 \times 10^{-9} \text{ } \Omega\text{m}$  and a mean free path  $l_e = \frac{R_Q/M}{(R-2R_c)/L} \simeq 200$  nm.

This resistivity is comparable to the  $4 \times 10^{-9} \text{ } \Omega\text{m}$  resistivity found in Ref. [18] in 70- to 90 nm-diameter-monocrystalline silver wires. The mean free path is 4 times the wire diameter, which attests to the quality of the nanowire, since in polycrystalline thin metal films the mean free path is usually smaller than the film thickness. However, it also points to the role of surfaces, the highly stressed core of the nanowires, and maybe twinning boundaries as additional scattering centers [19], since the bulk Ag resistivity is 30 times less.

The extrapolation to zero length yields a contact resistance of  $2 \text{ } \Omega$  for TiAl contacts (and thus  $\tau \simeq 0.2$ ), but this contact resistance varies from 0 to  $10 \text{ } \Omega$  depending on the contact material.

#### IV. FULL RANGE OF PROXIMITY EFFECT, FROM SHORT TO LONG JUNCTION

The superconducting proximity effect occurs at low enough temperature that the contacts are in the superconducting state, and that the Ag nanowire is quantum coherent over the entire segment length between two superconducting contacts. Andreev bound states, coherent superpositions of electron- and hole-like quasiparticles, then form in the normal metal, and can shuttle pairs from one superconductor to the other through the normal wire. This leads to a dissipationless supercurrent through the junction, whose maximum value is the critical current  $I_c$ .

In this section, we characterize the proximity effect in each junction by the switching current  $I_s$ , i.e., the current above which the S/Ag/S junction switches from nonresistive to resistive. This switching current can be smaller than  $I_c$ , which is calculated using the Usadel theory for SNS junctions, depending on the electromagnetic environment of the sample as well as the temperature. In particular, the reduction of  $I_c$  because of thermal fluctuations can be neglected if the Josephson energy  $E_J = \frac{\hbar}{2e} I_c$  is larger than temperature. An electronic temperature higher than the bath temperature would also reduce  $I_s$ . We are confident that such mechanisms are not at work in our experiments, for two reasons. Firstly, the switching currents we measure are high (above 100 nA), and secondly, we measure no saturation of the switching current as we decrease the temperature, implying that the electron temperature is not much higher than the bath temperature, thanks to the use of low pass dissipative filtering at room temperature, along the measurement lines and at the lowest temperature. We current bias the junction and use a standard lock-in technique to measure the differential resistance. The switching current is plotted as a function of segment length in Fig. 3(a).

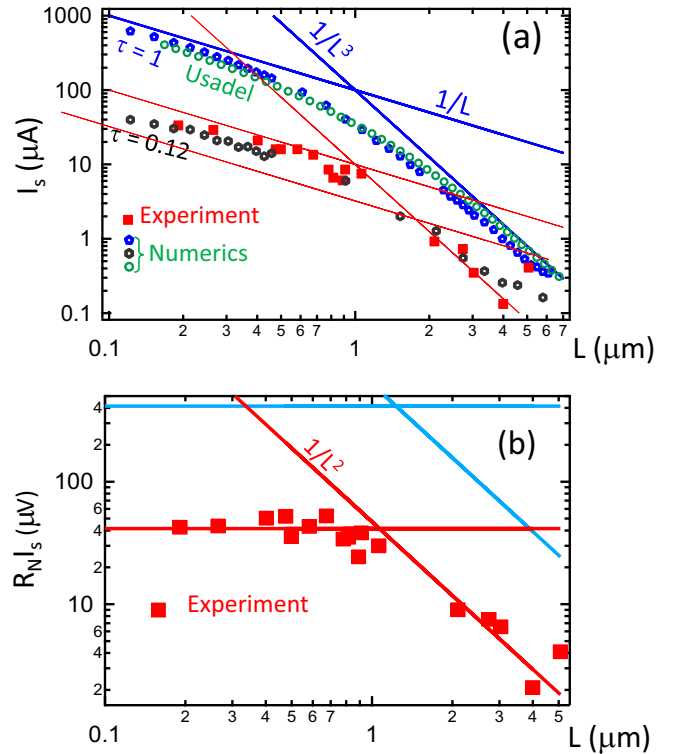


FIG. 3. Full range of the proximity effect, from short to long junction regime, in Ag nanowires with TiAl contacts. (a) Switching current as a function of length for the 17 segments (full red squares). Open black and blue symbols are the numerically calculated length dependence of the critical current of a diffusive SNS junction for interface transmissions  $\tau = 0.12$  and  $\tau = 1$ , respectively. Those results are obtained from the diagonalization of the Bogolubov-de Gennes Andreev spectrum of a tight-binding Hamiltonian on a square lattice with on-site disorder. Open green symbols are the results of the Usadel theory with perfect transmission, from Ref. [3]. In the simulations, the amplitude of the disordered potential and the superconducting gap were chosen such that  $l_e \simeq \xi_s/2 = 6a$  and the sample length was varied between  $L = 0.25\xi_s$  and  $30 \xi_s$ , which roughly corresponds to the experimental range. Interestingly, in this parameter range the Josephson current amplitude varies linearly with  $\tau$  down to  $\tau \simeq 10^{-2}$ . The transmission  $\tau = 0.12$  which can reproduce the experimental data is notably different from our estimate of  $\tau \in [0.23, 0.8]$  for the contact resistance to the Ag wire (see text). (b)  $R_N I_s$  as a function of length. The  $R_N I_s$  product is constant in the short junction regime, and decays as  $1/L^2$  in the long junction regime, as it should. (b) also compares the experimental values to theory for perfect transmission (blue lines) and demonstrates how the experimental values are systematically smaller. The crossover between short and long junction regimes, however, occurs at the predicted length.

Two regimes are clearly seen, that correspond to two different power-law dependencies of the switching current with length. The first is the regime of short junctions, in which the junction is shorter than the superconducting coherence length  $\xi_s^N = \sqrt{\hbar D_N / \Delta}$ , with  $D_N$  the diffusion constant in the Ag wire and  $\Delta$  the superconducting gap. Given the gap of Al  $\Delta \simeq 0.2$  meV and the diffusion parameters in Ag estimated earlier,  $D_N = v_F l_e / 3 = 0.032 \text{ m}^2/\text{s}$ , this yields  $\xi_s^N \simeq 0.36 \text{ } \mu\text{m}$ . In that

regime, the superconducting gap gives the energy scale of most phenomena. In the opposite regime of long junction, in which the junction is much longer than  $\xi_s$ , it is the Thouless energy  $E_{\text{Th}} = \hbar D_N/L^2$  that governs the physics. Given the relation  $R_N I_c \propto \min(\Delta, \hbar D_N/L^2)$ , in the diffusive regime the critical current scales as  $I_c \sim 1/L$  in the short junction limit, and  $I_c \sim 1/L^3$  for the long junction limit. These two different power laws are clearly displayed in Fig. 3(a). The crossover from short junction to long junction is located at  $L_{\text{cr}} = 1 \mu\text{m}$ , and is theoretically given by  $\sqrt{10.82 \hbar D_N/2.07 \Delta}$ , which is roughly twice the coherence length in the normal metal  $\xi_S^N = \sqrt{\hbar D_N/\Delta}$ . And indeed, the coherence length we extract from the crossover,  $\xi_S^{N,\text{exp}} = 0.43 \mu\text{m}$ , is close to the  $\xi_S^N \simeq 0.36 \mu\text{m}$  estimated above. Rather than plotting the switching current as a function of length, Fig. 3(b) plots the so-called junction “figure of merit,” or  $R_N I_s$  product, which, according to the theory of the proximity effect in the case of perfectly transparent contacts should be constant and equal to  $2.07 \Delta$  in the short junction regime, and to  $10.82 E_{\text{Th}} \simeq 1/L^2$  in the long junction regime [1–3]. The switching current [defined in Fig. 2(c)] shown in Fig. 3(b) qualitatively follows the theoretical prediction for  $I_c$ , both in terms of the length dependencies and the crossover length between short and long junction (around one micrometer). Quantitatively however, the measured  $R_N I_s$  is roughly five times smaller than the predicted  $R_N I_c$  in both limits.

This reduction is probably due to the imperfect transmission at the N/S interface, as explained in Ref. [20]. However, the reduction we find here, just like the reduction found in S/graphene/S junction [4], does not agree quantitatively with the prediction of the Usadel theory used in Ref. [20]. In the S/graphene/S case, the transmission deduced from the contact resistance was estimated to be  $\tau = 0.15 \pm 0.05$ . In the present case of Ag connected to TiAl contacts, the contact resistance of  $2R_c = 1.8 \pm 1 \Omega$  determined in the previous section, translates, given the roughly  $2 \times 10^4$  conduction channels in the nanowires, into  $\tau \in [0.23, 0.8]$ . As in Ref. [4], we have conducted tight binding simulations [21] of a few-channel diffusive wire connected to superconducting contacts, with varying interface transmission, for different wire lengths. We find that the reduction factor in  $R_N I_c$ , as well as the entire length dependence are well reproduced by the numerical calculations for a transmission of 0.12, as shown in Fig. 3(a). This transmission is significantly smaller than the smallest value compatible with the measured contact resistance. Therefore, in addition to a bad contact transmission (typical of contacts between metals and semiconductors or carbon-based materials such as graphene), other physical mechanisms are needed to explain the reduction of  $R_N I_c$ . One possibility is a reduced induced superconductivity due to the small size of the superconducting Al contacts with respect to the superconducting coherence length of Al films:  $\xi_{\text{Al}} = \sqrt{\xi_{0,\text{Al}} l_{e,\text{Al}}} \simeq 600 \text{ nm}$  where  $\xi_{0,\text{Al}} = \hbar v_F/\Delta_{\text{Al}} \simeq 5 \mu\text{m}$  is the coherence length of clean Al, and  $l_{e,\text{Al}}$  is estimated using a thickness-limited mean free path in our Al films  $l_{e,\text{Al}} = t = 75 \text{ nm}$ . Another possibility is the effect of out-of-equilibrium quasiparticles in the aluminum contacts. Their strong influence on the field-dependence of the switching current will be discussed in the next section. We note that such a discrepancy

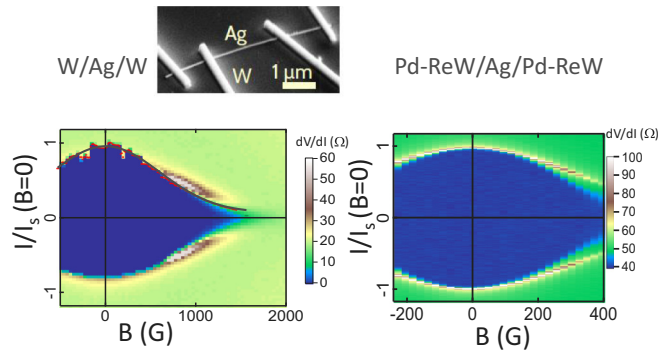


FIG. 4. Absence of magnetic field-induced reentrance for Ag nanowires connected to superconductors other than Al. (Left) Color-coded four-wire differential resistance of a W/Ag/W junction of length  $2 \mu\text{m}$  (SEM image inset), as a function of dc current (vertical axis, renormalized by the maximum switching current of  $0.288 \mu\text{A}$ ) and magnetic field (horizontal axis). The field dependence of both the switching and retrapping currents is monotonous and Gaussian-like, as theoretically expected for a unidimensional geometry. The continuous line is a Gaussian fit to the field-dependence of the extracted switching current (red points). Right, color-coded differential resistance of the two-wire differential resistance of a  $900\text{-nm}$ -long Ag segment connected to superconducting Pd-ReW electrodes. The current on the vertical axis is renormalized by the maximum switching current of  $3.08 \mu\text{A}$ . Both the switching and retrapping current vary monotonously with magnetic field (the bias current is swept from negative to positive in these plots).

between calculated and measured  $R_N I_c$  was not observed in Al/Au/Al junctions measured by Angers *et al.* [22], in which the Al wires had a larger section and the S/N contact area was much larger.

## V. FIELD DEPENDENCE OF THE PROXIMITY EFFECT: STANDARD GAUSSIAN DECAY IN MOST JUNCTIONS AND SURPRISING REENTRANCE FEATURES IN Al/Ag/Al JUNCTIONS

The effect of a magnetic field on an SNS junction depends on the junction geometry, specifically on the aspect ratio of the N part. Whereas wide two-dimensional-like junctions exhibit a nonmonotonous, Fraunhofer-like critical current versus field pattern, narrow one-dimensional-like junctions display a monotonous, Gaussian-like decay with field of the critical current [9–11]. Such monotonous decays are demonstrated in Fig. 4, for a Ag nanowire connected to FIB-grown W electrodes and a Ag nanowire connected to ReW electrodes. This type of field dependence was previously reported in 1D Nb/Au/Nb SNS junctions where the Au nanowires were made of polycrystalline thin films [10].

In striking contrast, the field dependence of the switching current through S/Ag/S junctions with Al contacts, measured in four-wire (4W) configuration, displayed in Fig. 5, is non-monotonous. It first increases with field, then decreases in a Gaussian manner above about  $150 \text{ G}$ . One of the main results of this paper is that all junctions with Al contacts display such a behavior, as also shown in the Appendix. This reentrant behavior was also reported previously for Al/Au/Al junctions (but not Nb/Au/Nb junctions), with a relative 10% effect, in

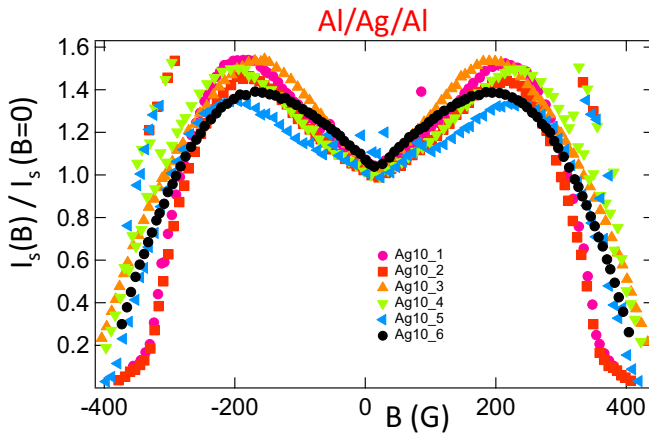


FIG. 5. Magnetic field-induced reentrant switching current of six Al/Ag/Al junctions, measured in a four-wire configuration. The spurious points around  $\pm 300$  G are due to the numerical extraction procedure of  $I_s$  from plots of the differential resistance as a function of bias current and magnetic field.

which the Au wires were made of polycrystalline thin films, roughly 100 nm wide and 1200 to 1500 nm long [22].

To investigate this intriguing behavior of the Al/Ag/Al junctions, we compared two-wire and four-wire measurements of a given junction. Figure 6 displays the differential resistance versus current and magnetic field of a given junction in two different configurations. The first is a four-wire configuration, shown in Fig. 6(a), in which the current is injected via the Ag nanowire outside the segment, and the voltage drop is recorded between the superconducting probes connecting the segment. The reentrant feature is clear, both in the switching and retrapping current. It is also notable that in this four-wire configuration, the switching current (the current above which the resistance goes from zero to the normal state value) is the same as the retrapping current (the current below which the resistance goes from the normal state value to zero). By contrast, in the two-wire configuration, shown in Fig. 6(b), the same, superconducting, electrodes are used to inject the current and to measure the voltage drop. Strikingly, only the retrapping current displays a reentrance in that case, and the switching current is higher than the retrapping current.

This behavior recalls that of field-enhanced superconductivity seen in extremely narrow (less than 10 nm) superconducting wires of amorphous MoGe and Nb [23,24]. Field enhanced superconductivity is attributed to the beneficial effect of the magnetic field in freezing out the spin of magnetic impurities, which in zero field act as inelastic scattering centers and decrease the critical current. We believe that the mechanism at play in our case of SNS junctions is different since magnetic impurities are Kondo screened in Al [25]. Moreover, we found no field-enhanced superconductivity (field reentrance) in test Al wires of the same thickness and width (170 nm) as the Al contacts used in the S/Ag/S junctions that displayed the anomalous field reentrance, as shown in Fig. 7.

A qualitative description of the physics that could be at work is suggested by the difference between the two-wire and four-wire measurement. In the four-wire configuration, the

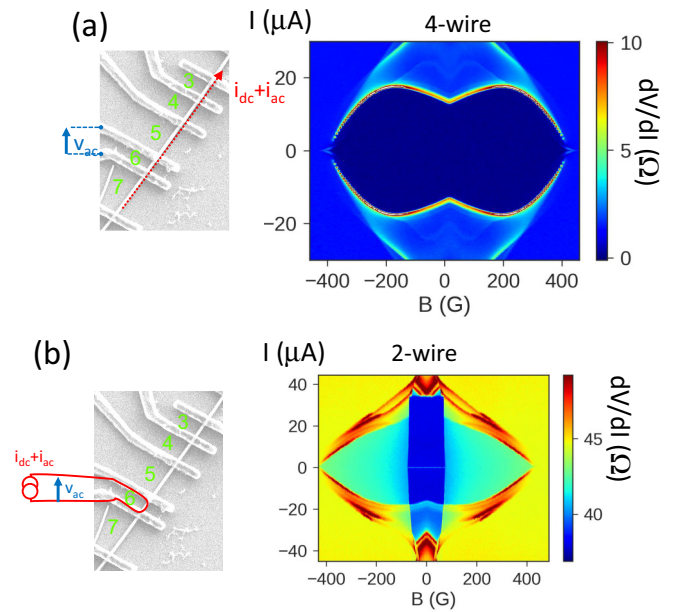


FIG. 6. Color-coded differential resistance  $dV/dI = v_{ac}/i_{ac}$  of segment Ag10-6 with TiAl electrodes, in four-wire (a) and two-wire (b) measurements, as a function of dc current and magnetic field. In the four-wire configuration, the switching current is equal to the retrapping current, indicating sample heating, even as supercurrent runs through the junction, and the reentrant feature with magnetic field is clear. By contrast, in the two-wire configuration, the switching current at low field is up to twice the retrapping current, indicating that the sample is better thermalized. The retrapping currents are the same in both configurations, as expected since the retrapping current is determined by the heating due to the segment having switched to the resistive state, see text. The two-wire resistance measures all leads up to the macroscopic bonding pads, so that the critical field  $H_{c,b}$  of the bulk contact pads is visible at 75 G, which corresponds to one flux quantum through an area of size  $\xi_{Al}^2$ , and the proximity effect disappears at the critical field of the electrodes, 400 G, which corresponds to one flux quantum through an area of size  $\xi_{Al}W$ , where  $W = 170$  nm is the Al electrode width.

current is injected via the Ag nanowire. It is thus possible that there is a nonfully proximitized region in that wire outside the segment being measured. That would cause not only paired electrons but also hot quasiparticles to be injected in the Ag section we measure. In zero field, those quasiparticles could not relax, in particular due to the hard superconducting gap of the Al electrodes, and would thus “poison” the junction, causing the switching current to be smaller. A magnetic field however softens the superconducting gap, i.e., induces some quasiparticle density of states in the gap, so the injected quasiparticles could thermalize in the superconducting electrodes at lower temperature than at zero field, which would increase the critical current. A similar mechanism could explain the field dependence of the retrapping current, since the retrapping current depends on the cooling possibilities of hot quasiparticles [26].

We note that the behavior we describe, in which a supercurrent runs through the junction and yet dissipation occurs, which decreases the switching current, is different from the situation addressed in Ref. [26], in which dissipation occurs

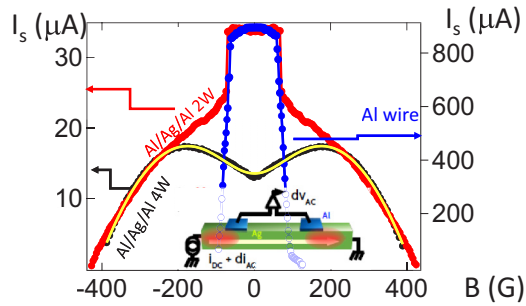


FIG. 7. Comparison of the switching current of segment Ag10-6 with TiAl electrodes, in four-wire (black curve) and two-wire (red curve) measurement, with the switching current of an Al wire of same dimensions as the TiAl electrodes used to contact the Ag wires (blue curve, vertical scale on the right). No reentrant behavior is observed in the Al wire field dependence, indicating that the reentrance is a feature of the proximity effect and not of the sole Al nanowire. The sharp cutoff starting around 75 G corresponds to the bulk Al's critical field  $H_{c,b}$ , given by one flux quantum through an area of  $(500 \text{ nm})^2$ , in accordance with the superconducting coherence length of a disordered aluminum thin film (estimated in the text). The yellow curve is the fit of the four-wire measurement to expression (B2) of the Appendix describing the field-reentrance behavior.

once the junction has switched to a resistive state, which leads to a decrease of the retrapping current below the value of the switching current. The heating addressed here leads to a switching current whose value is decreased below the switching current of the same segment measured in a two-wire configuration (see Figs. 6 and 7), in some cases to a value equal to the retrapping current.

In the Appendix, we propose a model of how the Joule power dissipated in a small normal portion of the Ag wire reduces the switching current, by equating the heat produced with the reduction of Josephson energy. The fit using this model is shown in Fig. 7, and describes the data well.

In contrast with the four-wire switching current, the switching current in the two-wire configuration, in which the current is injected in the Ag segment via superconducting Al electrodes, is maximum at zero magnetic field. It jumps down at 75 G, the critical field  $H_{c,b}$  of the bulk contact pads, as visible in the (roughly 1 mA) critical current of an Al wire of similar dimensions, see Fig. 7. This jump is followed at higher field by a smooth parabolic decay which coincides above 200 G with the field dependence of the four-wire configuration. Both switching currents (two- and four-wire configurations) go to zero above 400 G, the critical field of the 100-nm-wide aluminum electrodes that contact the Ag wires. Since the Al bulk contact pads are more than several hundred microns away from the SNS junctions, it is surprising that their field transition should influence the switching current. Our understanding is that the switching current decreases above  $H_{c,b}$  because hot quasiparticles are generated in the normal part of the bulk electrode and injected in the narrow part which is still superconducting.

It is interesting that the two configurations have strikingly different magnetic field dependencies, even though both behaviours are due to hot quasiparticles generated in the aluminum electrodes. The difference is due to the fact that

the quasiparticles are generated either in the bulk electrodes (two-probe configuration) or close to the NS interface (four-probe configuration). The strong effect of these quasiparticles is due to the uncommonly small inelastic electron-phonon scattering rate in Al at low temperature [27], which implies that cooling is controlled by the quasiparticles in aluminum. We note that the reentrance does not only occur in the four-wire configuration for which the current is injected through a longer segment with a smaller switching current than the measured segment: although we have not tested all possible configurations, we have seen the reentrance in all four-wire configurations we measured, including when the current was injected via a segment with a higher switching current than the measured segment, suggesting that this effect is a general feature of nanowires connected to aluminum contacts. We also believe that the reentrance should be most striking in 1D-like geometries (long and narrow segments) rather than wider, 2D-like geometries with greater quasiparticle thermalization (see the absence of reentrance in Refs. [28,29]). The effect is also expected to be greatest in narrow Al electrodes, since the gap could be less hard, and therefore more prone to quasiparticle states being induced by the magnetic field.

Finally, we suggest that the behavior we have described and its explanation may apply to the field-induced switching current enhancement recently reported in InAs nanowires similarly connected to aluminum electrodes [13]. Although the authors attributed this enhancement to a topological transition, and the enhancement is more abrupt, the typical field and relative amplitude of the enhancement are similar, suggesting a possible similar cause.

## VI. CONCLUSION

We have presented an extensive investigation of Ag nanowire-based Josephson junctions, with aluminum as the superconducting material, from the short to the long junction regime. Our experiments, and specifically the unusual field dependence of the switching current, strikingly demonstrate the importance of the thermalization of quasiparticles at the NS interface in systems where thermalization must proceed through aluminum electrodes. This work is particularly relevant in the context of topological superconductivity and the intensively investigated configurations in which nanowires with high spin-orbit are connected to superconducting electrodes, in which topological transitions with magnetic fields are predicted. It is also relevant to the more general phenomenon of quasiparticle poisoning, whose field dependence may need to be taken into account [14].

## ACKNOWLEDGMENTS

We acknowledge Mathieu Kociak for the TEM imaging, Meydi Ferrier for insightful suggestions on the manuscript and funding from ANR of projects MASH (ANR-12-BS04-0016), MAGMA (ANR-16-CE29-0027), JETS (ANR-16-CE30-0029), and DIRACFORMAG (ANR-14-CE32-0003), and Labex PALM.

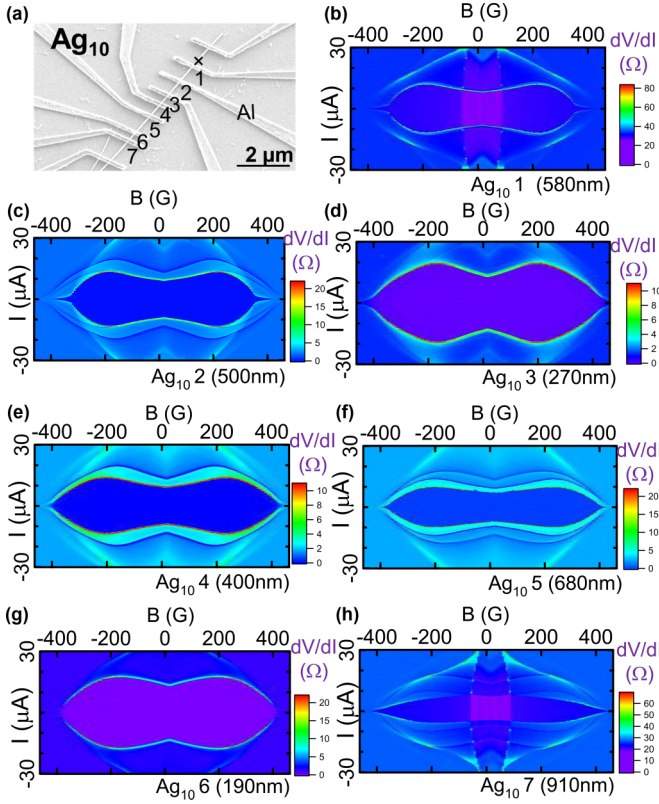


FIG. 8. Color-coded differential resistance of seven segments from wires  $\text{Ag}_{10}$ , connected to TiAl electrodes, as a function of bias current and magnetic field. Segments 1 and 7 are measured in a three-wire configuration, segments 2 to 6 are measured in a four-wire configuration. The reentrant field dependence is clear.

#### APPENDIX A: FIELD AND CURRENT DEPENDENCE OF SEVEN SEGMENTS OF Ag WIRES CONNECTED TO TiAl ELECTRODES

The colour-coded differential conductance as a function of current and magnetic field of seven segments of wire  $\text{Ag}_{10}$ , connected to TiAl electrodes, is displayed in Fig. 8. The switching currents plotted in Fig. 5 of the main text are extracted from these plots.

#### APPENDIX B: MODEL FOR FIELD REENTRANCE OF SWITCHING CURRENT

In the following, we propose a model of how the Joule power dissipated in a small normal portion of the Ag wire reduces the switching current, by equating the heat produced with the reduction of Josephson energy.

We assume that a small normal part in the Ag wire near the Al contact causes Joule heating with power  $R_{\text{qp}}i(B)^2$ . This power is converted over the quasiparticle thermalization time  $\tau_{\text{qp}}$ , into an energy that reduces the Josephson energy:

$$R_{\text{qp}}i^2(B)\tau_{\text{qp}} = \phi_0(i_0(B) - i(B)), \quad (\text{B1})$$

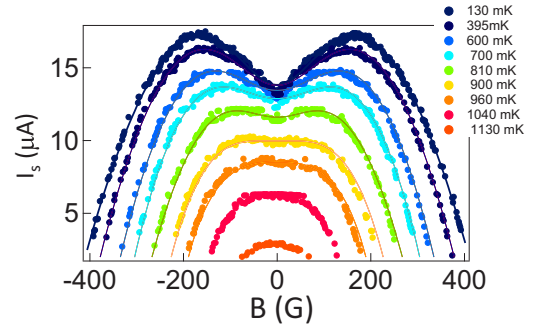


FIG. 9. Variations with temperature of the reentrant feature in the switching current versus field curves of segment  $\text{Ag}_{10-6}$ . In accordance with our understanding of the nonmonotonous field dependence of the switching current as due to the heating effects of injected quasiparticles, the reentrance amplitude decreases as the sample temperature increases, since the cooling power of phonons increases with temperature. The experimental curves (markers) are taken at temperatures between 130 and 1130 mK, as indicated. Fits of the curves to equation (B2) are plotted as continuous lines. The curve shape is well described by the model, although the lowest temperature curves display a somewhat sharper zero field cusp than described by the model.

where  $\tau_{\text{qp}}$  is the characteristic electron-electron interaction time, and  $\phi_0 = \hbar/2e$ . The solution is

$$i(B) = \frac{\phi_0}{2R_{\text{qp}}} \frac{1}{\tau_{\text{qp}}(B)} \left( -1 + \sqrt{1 + 4 \frac{R_{\text{qp}}}{\phi_0} i_0(B)\tau_{\text{qp}}(B)} \right). \quad (\text{B2})$$

Here,  $i_0(B)$  is the critical current that would be measured with no Joule effect. Its decay with magnetic field is due to both the field-induced depairing in the superconducting contacts, and the field-dependent decay of the supercurrent through an

TABLE I. Parameters of the proximity effect induced in one segment of wire  $\text{Ag6}'$  and three segments of wire  $\text{Ag6}$ , displayed on the SEM image of Fig. 2(b). The two wires  $\text{Ag6}$  and  $\text{Ag6}'$  were on the same chip, and connected to TiAl electrodes in the same deposition step.

Segment	$\text{Ag6}'\text{-KM}$	$\text{Ag6}\text{-DU}$	$\text{Ag6}\text{-DZ}$	$\text{Ag6}\text{-ZX}$
Material	TiAl	TiAl	TiAl	TiAl
$\Delta$ ( $\mu\text{eV}$ )	200	200	200	340
Length ( $\mu\text{m}$ )	0.78	1.06	5.07	0.89
$R_{\text{tot}}$ ( $\Omega$ )	4	4	10	4
$R_c$ ( $\Omega$ )	$1.8 \pm 1$	$1.8 \pm 1$	$1.8 \pm 1$	$1.8 \pm 1$
$R_N$ ( $\Omega$ )	1.30	1.30	7.30	1.30
$I_c$ ( $\mu\text{A}$ )	8.5	7.5	0.39	6.1
$eR_N I_c$ ( $\mu\text{eV}$ )	34	30	3.9	24.4
$eR_N I_c / \Delta$	0.17	0.15	0.02	0.07
$E_{\text{Th}}$ ( $\mu\text{eV}$ )	32.36	17.52	0.77	24.85
$10.82E_{\text{Th}} / \Delta$	1.75	0.95	0.04	0.79
$k_B T / E_{\text{Th}}$	0.29	0.54	12.31	0.38
$eR_N I_c / E_{\text{Th}}$	1.05	1.71	5.09	0.98
$\xi$ (nm)	313	313	313	313
$L / \xi$	2.49	3.39	16.20	2.84
$R_c / 2R_N$	1.04	1.04	0.18	1.04

SNS junction [10,30]. A simple approximation is

$$i_0(B) = i_0(0) \left( 1 - \left( \frac{B}{B_0} \right)^2 \right), \quad (\text{B3})$$

where  $B_0$  is the characteristic magnetic field of the decay. The quasiparticle thermalization rate, in contrast, increases with magnetic field, as the quasiparticle density of states in the superconductor increases. The simplest approximation is to take a rate proportional to the square of the magnetic field,

$$\tau_{\text{qp}}(B)^{-1} = \tau_{\text{qp}}(0)^{-1} \left( 1 + \left( \frac{B}{B_1} \right)^2 \right). \quad (\text{B4})$$

A fit to the data is shown in Fig. 9, and qualitatively describes the data well. The fit parameters are  $B_0 = 415$  G, the high

field decay scale of the supercurrent;  $B_1 = 106$  G, the field scale over which the quasiparticle thermalization time varies with field, leading to the reentrant part of the curve (positive  $i(B)$  slope);  $i_0 = 30.3$   $\mu\text{A}$  and  $\frac{\phi_0}{2R_{\text{qp}}\tau_{\text{qp}}(0)} = 10.95$   $\mu\text{A}$ . Since the zero field thermalization time  $\tau_{\text{qp}}(0)$  is about  $1-10 \times 10^{-9}$  s in Al [27], this yields  $R_{\text{qp}} \simeq 0.1$   $\Omega$  as the value of the resistance causing the Joule power dissipation.

### APPENDIX C: PARAMETERS OF TiAl/Ag/TiAl JUNCTIONS ON WIRES Ag6 AND Ag6'

The parameters of four TiAl/Ag/TiAl junctions are given in Table I.

- 
- [1] I. O. Kulik and A. N. Omel'yanchuk, Contribution to the microscopic theory of the Josephson effect in superconducting bridges, *Zh. Eksp. Teor. Fiz. Pis. Red.* **21**, 216 (1975) [*JETP Lett.* **21**, 96 (1975)].
- [2] K. K. Likharev, Superconducting weak links, *Rev. Mod. Phys.* **51**, 101 (1979).
- [3] P. Dubos, H. Courtois, B. Pannetier, F. K. Wilhelm, A. D. Zaikin, and G. Schon, Josephson critical current in a long mesoscopic S-N-S junction, *Phys. Rev. B* **63**, 064502 (2001).
- [4] C. Li, S. Guéron, A. Chepelianskii, and H. Bouchiat, Full range of proximity effect probed with superconductor/graphene/superconductor junctions, *Phys. Rev. B* **94**, 115405 (2016).
- [5] C. T. Ke, C. M. Moehle, F. K. de Vries, C. M. Moehle, F. K. de Vries, C. Thomas, S. Metti, C. R. Guinn, R. Kallaher, M. Lodari, G. Scappucci, T. Wang, R. E. Diaz, G. C. Gardner, M. J. Manfra, and S. Goswami, Ballistic superconductivity and tunable  $\tilde{I}$ junctions in InSb quantum wells, *Nat. Commun.* **10**, 3764 (2019).
- [6] D. Toybou, C. Celle, and C. Aude-Garcia, Thierry Rabilloud and Jean-Pierre Simonato, A toxicology-informed, safer by design approach for the fabrication of transparent electrodes based on silver nanowires, *Environ. Sci.: Nano* **6**, 684 (2019).
- [7] Z. Cheng, L. Liu, S. Xu, M. Lu, and X. Wang, Temperature dependence of electrical and thermal conduction in single silver nanowire, *Sci. Rep.* **5**, 10718, (2015).
- [8] D. Langley, G. Giusti, C. Mayousse, C. Celle, D. Bellet, and J.-P. Simonato, Flexible transparent conductive materials based on silver nanowire networks: a review, *Nanotechnology* **24**, 452001 (2013).
- [9] G. Montambaux, Interference pattern of a long diffusive Josephson junction, [arXiv:0707.0411](https://arxiv.org/abs/0707.0411).
- [10] F. Chiodi, M. Ferrier, S. Guéron, J. C. Cuevas, G. Montambaux, F. Fortuna, A. Kasumov, and H. Bouchiat, Geometry-related magnetic interference patterns in long SNS Josephson junctions, *Phys. Rev. B* **86**, 064510 (2012).
- [11] J.-C. Cuevas and F. S. Bergeret, Magnetic Interference Patterns and Vortices in Diffusive SNS Junctions, *Phys. Rev. Lett.* **99**, 217002 (2007).
- [12] S. Abay, D. Persson, H. Nilsson, F. Wu, H. Q. Xu, M. Fogelstrom, V. Shumeiko, and P. Delsing, A similar geometry of S/InAs-nanowire/S junctions was explored in Charge transport in InAs nanowire Josephson junctions, *Phys. Rev. B* **89**, 214508 (2014).
- [13] J. Tiira, E. Strambini, M. Amado, S. Roddaro, P. San-Jose, R. Aguado, F. S. Bergeret, D. Ercolani, L. Sorba, and F. Giazotto, Magnetically-driven colossal supercurrent enhancement in InAs nanowire Josephson junctions, *Nat. Commun.* **8**, 14984 (2017).
- [14] S. M. Albrecht, E. B. Hansen, A. P. Higginbotham, F. Kuemmeth, T. S. Jespersen, J. Nygård, P. Krogstrup, J. Danon, K. Flensberg, and C. M. Marcus, Transport Signatures of Quasiparticle Poisoning in a Majorana Island, *Phys. Rev. Lett.* **118**, 137701 (2017); M. Zgirski, L. Bretheau, Q. Le Masne, H. Pothier, D. Esteve, and C. Urbina, Evidence for Long-Lived Quasiparticles Trapped in Superconducting Point Contacts, *ibid.* **106**, 257003 (2011).
- [15] C. Li, A. Kasumov, A. Murani, S. Sengupta, F. Fortuna, K. Napolskii, D. Koshkodaev, G. Tsirlina, Y. Kasumov, I. Khodos, R. Deblock, M. Ferrier, S. Guéron, and H. Bouchiat, Magnetic field resistant quantum interferences in Josephson junctions based on bismuth nanowires, *Phys. Rev. B* **90**, 245427 (2014).
- [16] Yu. V. Sharvin, A possible method for studying Fermi surfaces, *Zh. Eksp. Teor. Fiz.* **48**, 984 (1965) [*Sov. Phys. JETP* **21**, 655 (1965)].
- [17] Datta, *Electronic Transport in Mesoscopic Systems* (Cambridge University Press, Cambridge, UK, 1995).
- [18] M. M. Kolečnik-Gray, S. Hansel, M. Boese, and V. Krstić, Impact of surface and twin-boundary scattering on the electrical transport properties of Ag nanowires, *Solid State Commun.* **202**, 48 (2015).
- [19] A. Bid, A. Bora, and A. K. Raychaudhuri, Temperature dependence of the resistance of metallic nanowires of diameter  $\geq 15$  nm: Applicability of Bloch-Grüneisen theorem, *Phys. Rev. B* **74**, 035426 (2006).
- [20] J. C. Hammer, J. C. Cuevas, F. S. Bergeret, and W. Belzig, Density of states and supercurrent in diffusive SNS junctions: Roles of nonideal interfaces and spin-flip scattering, *Phys. Rev. B* **76**, 064514 (2007).
- [21] A. Murani, A. Chepelianskii, S. Guéron, and H. Bouchiat, Andreev spectrum with high spin-orbit interactions: Revealing spin splitting and topologically protected crossings, *Phys. Rev. B* **96**, 165415 (2017).

- [22] L. Angers, F. Chiodi, G. Montambaux, M. Ferrier, S. Guéron, H. Bouchiat, and J. C. Cuevas, Proximity dc squids in the long-junction limit, *Phys. Rev. B* **77**, 165408 (2008).
- [23] A. Rogachev, T.-C. Wei, D. Pekker, A. T. Bollinger, P. M. Goldbart, and A. Bezryadin, Magnetic-Field Enhancement of Superconductivity in Ultranarrow Wires, *Phys. Rev. Lett.* **97**, 137001 (2006).
- [24] M. Yu. Kharitonov and M. V. Feigel'man, Enhancement of superconductivity in disordered films by parallel magnetic field, *JETP Lett.* **82**, 421 (2005).
- [25] N. Ashcroft and N. Mermin, *Solid State Physics* (Saunders College, Rochester, NY, 1976), Chap. 32.
- [26] H. Courtois, M. Meschke, J. T. Peltonen, and J. P. Pekola, Origin of Hysteresis in a Proximity Josephson Junction, *Phys. Rev. Lett.* **101**, 067002 (2008).
- [27] P. Santhanam and D. E. Prober, Inelastic electron scattering mechanisms in clean aluminum films, *Phys. Rev. B* **29**, 3733 (1984).
- [28] H. A. Nilsson, P. Samuelsson, P. Caroff, and H. Q. Xu, Supercurrent and multiple Andreev reflections in an InSb nanowire Josephson junction, *Nano Lett.* **12**, 228 (2011).
- [29] A. Fornieri, A. M. Whiticar, F. Setiawan, E. Portolés, A. Drachmann, A. Keselman, S. Gronin, C. Thomas, T. Wang, R. Kallaher, G. C. Gardner, E. Berg, M. J. Manfra, A. Stern, C. M. Marcus, and F. Nichele, Evidence of topological superconductivity in planar Josephson junctions, *Nature (London)* **569**, 89 (2019); F. Nichele, E. Portolés, A. Fornieri, A. M. Whiticar, A. C. C. Drachmann, T. Wang, G. C. Gardner, C. Thomas, A. T. Hatke, M. J. Manfra, and C. M. Marcus, Relating Andreev Bound States and Supercurrents in Hybrid Josephson Junctions, *Phys. Rev. Lett.* **124**, 226801 (2020).
- [30] A. Anthore, H. Pothier, and D. Esteve, Density of States in a Superconductor Carrying a Supercurrent, *Phys. Rev. Lett.* **90**, 127001 (2003).